Suppressing transition metal dissolution and deposition in lithium-ion batteries using oxide solid electrolyte coated polymer separator*

Zhao Yan(闫昭)[1,2], Hongyi Pan(潘弘毅)[1,2], Junyang Wang(汪君洋)[1,2], Rusong Chen(陈汝颂)[1,2], Fei Luo(罗飞)[4], Xiqian Yu(禹习谦)[1,2,3,‡], and Hong Li(李泓)[1,2,3,†]

[1] *Beijing Advanced Innovation Center for Materials Genome Engineering, Institute of Physics, Chinese Academy of Sciences, Beijing* 100190, *China*
[2] *School of Physical Sciences, University of Chinese Academy of Sciences, Beijing* 100049, *China*
[3] *Yangtze River Delta Physics Research Center Co., Ltd., Liyang* 213300, *China*
[4] *Tianmulake Excellent Anode Materials Co., Ltd., Liyang* 213300, *China*

(Received 21 April 2020; revised manuscript received 8 May 2020; accepted manuscript online 25 May 2020)

The dissolution of transition metal (TM) cations from oxide cathodes and the subsequent migration and deposition on the anode lead to the deconstruction of cathode materials and uncontrollable growth of solid electrode interphase (SEI). The above issues have been considered as main causes for the performance degradation of lithium-ion batteries (LIBs). In this work, we reported that the solid oxide electrolyte $Li_{1.5}Al_{0.5}Ti_{1.5}(PO_4)_3$ (LATP) coating on polyethylene (PE) polymer separator can largely block the TM dissolution and deposition in LIBs. Scanning electron microscopy (SEM), second ion mass spectroscopy (SIMS), and Raman spectroscopy characterizations reveal that the granular surface of the LATP coating layer is converted to a dense morphology due to the reduction of LATP at discharge process. The as-formed dense surface layer can effectively hinder the TM deposition on the anode electrode and inhibit the TM dissolution from the cathode electrode. As a result, both the $LiCoO_2$/SiO-graphite and $LiMn_2O_4$/SiO-graphite cells using LATP coated PE separator show substantially enhanced cycle performances compared with those cells with Al_2O_3 coated PE separator.

Keywords: transition metal dissolution, cathode, lithium-ion batteries, solid electrolyte, separator

PACS: 82.47.Aa, 62.23.Pq, 65.40.gk **DOI:** 10.1088/1674-1056/ab9610

1. Introduction

Lithium-ion batteries (LIBs) achieve excellent performances such as high energy density and long cycle lifespan, and have been put into applications in consumer electronics, electric vehicles, and grid-scale energy storage for decades.[1–3] Notwithstanding the great progresses that have been made in LIBs materials and battery technologies, the common cathode materials used in commercial LIBs still have numerous intractable issues that restrict the further improvement of the battery performances. One of the most arresting problems is the dissolution of transition metal (TM) cations from cathode materials, especially for layered oxide cathodes $LiTMO_2$ (TM = Ni, Co, Mn, etc.),[4–7] which significant impacts the battery performances. Explicitly, the dissolution of TM over the battery cycling process leads to deconstruction of the cathode materials and diminish of the valence-variable TM, resulting in capacity fade of the cathodes.[8,9] Meanwhile, the dissolved TM cations can migrate and deposit on the anode electrode, and subsequently catalyze the decomposition of the electrolyte, leading to uncontrollable growth of solid electrolyte interphase (SEI) and thus deterioration of the interfacial properties,[10–12] which synergistically contribute to the performance degradation of LIBs.

Numerous previous studies have revealed that the TM dissolution issue is affected by various intertwined factors, such as bulk structure and surface chemistry of cathode, electrolyte, and additives, battery testing protocols and conditions. Accordingly, plenty of strategies and methods have been proposed and developed to address the TM dissolution issue from different aspects. Bulk doping[13,14] and surface coating[15,16] on cathode materials are the most widely used methods that are expected to intrinsically improve the structural stability of the material against TM dissolution. Electrolyte additives have been demonstrated to be highly effective to enable the formation of a stable SEI or cathode electrolyte interface (CEI) layer that can physically separate the cathode and electrolyte, and thus prevent the side reaction induced TM dissolution.[17,18] Employing polycation chelating agents to capture TM ion has also been reported to address the TM dissolution issue. Although this method cannot directly prevent the TM dissolution, the capture of TM and the restrained deposition on the anode can prevent the undesired side reactions between the anode and electrolyte, and thus resulting in enhanced cycle stability.[19] Recently, coating functional materials onto the polymer separator has been considered as an alternative way to solve the TM dissolution issue.[6,19] For example, it is reported

*Project supported by the National Key R&D Program of China (Grant No. 2016YFB0100100) and the National Natural Science Foundation of China (Grant Nos. 51822211, U1932220, U1964205, and U19A2018).

†Corresponding author. E-mail: hli@iphy.ac.cn
‡Corresponding author. E-mail: xyu@iphy.ac.cn

that the coating of $CaCO_3$ can consume HF in the electrolyte and thus avoid its reaction with the cathode. All these methods have demonstrated the effectiveness of inhibiting the TM dissolution and thus can greatly improve the battery performances.

In the present work, the oxide solid electrolyte $Li_{1.5}Al_{0.5}Ti_{1.5}(PO_4)_3$ (LATP), which delivers high ionic conductivity and has a reasonable cost, was employed to be coated on the polyethylene (PE) separator.[20] The LATP coated PE separator was proposed to inhibit the deterioration of battery performances resulted from TM dissolution. Microscopic and spectroscopic characterizations revealed the significant changes of the LATP surface morphology owing to the reduction of LATP during battery cycling. The as-formed compact surface layer can effectively block the TM ion from getting to the anode electrode for the subsequent deposition, and in the meantime inhibit the TM dissolution from the cathode, leading to the enhanced interfacial stability as well as the cathode structure stability. Accordingly, the $LiCoO_2$/silicon monoxide (SiO)-graphite and $LiMn_2O_4$/SiO-graphite cells using the LATP coated separator show superior cycle performances to the cells using regular Al_2O_3 coated separator.

2. Experiment

2.1. Preparation of the LATP coated PE separator and the Al_2O_3 coated PE separator

The synthesis of nanoscale LATP was reported in our previous work.[21] A coating slurry was prepared by dissolving 4 g polyvinylidene fluoride (PVDF, HSV900, Arkema) in 80 g N-methyl-2-pyrrolidone (NMP) solvent, followed by dispersing 16 g LATP particles into the solution through vigorous stirring. Then, the coating slurry was uniformly spread onto the PE separator (ND12, Shanghai Energy New Material Technology Co.) and transferred into the 100 ℃ oven to remove the solvent. After 12 hours, the one-side-coated separator (LATP@PE) was obtained. The Al_2O_3 coated PE separator (Al_2O_3@PE) was prepared following the same procedures. Commercial Al_2O_3 with particle size of around 500 nm (99.99%, Sigma-Aldrich) was used.

2.2. Material characterizations

The x-ray powder diffraction (XRD) was performed on a D8 Advance diffractometer (Bruker, D8 ADVANCE) with Cu $K\alpha$ radiation. The 2θ scan range was from 10° to 80° with a step size of 0.05°. The morphologies of the LATP, LATP@PE, and Al_2O_3@PE were characterized by a scanning electron microscopy (SEM, S-4800, Hitachi). Pre-decomposition of the gold layer (5 nm) was conducted to enhance the surface electronic conductivity and thus improve the contrast of the images. The element content was measured by a second ion mass spectroscopy (SIMS, HIDEN ANALYTICAL) with an Ar-ion beam current of 300 nA. Raman spectra were collected using a Renishaw 2000 system (Renishaw, UK) with an argon-ion laser (514.5 nm). For all post-analysis of the cycled electrode, the samples were retrieved from the cell and carefully washed by DMC, followed by a vacuum-drying process to remove the solvent. All samples were transferred with a protection box filled with high purity argon gas to avoid air contamination.

2.3. Electrode preparation

The $LiCoO_2$ (LCO) or $LiMn_2O_4$ (LMO) cathode electrodes contain active cathode material, super P, and PVDF with a mass ratio of 8 : 1 : 1. The specific capacity of the LCO/LMO cathode is 3.2 mAh/cm^2. The mass loadings of the LCO and LMO cathodes are 22.2 mg/cm^2 and 36.4 mg/cm^2, respectively. The diameter of the LCO/LMO cathode piece is 12 mm. For the anode electrode, SiO/graphite composites with controlled capacities of 400 mAh/g and 650 mAh/g were used to pair with the $LiCoO_2$ and $LiMn_2O_4$ cathodes, denoted as SOC400 and SOC650, respectively. The SOC400/SOC650 anode electrodes contain the active materials, super P, carboxymethyl cellulose (CMC), and styrene-butadiene rubber (SBR) with a mass ratio of 7 : 1 : 1 : 1. The specific capacity of the anode is 3.5 mAh/cm^2. The mass loadings of the SOC400 and SOC650 anodes are 10.9 mg/cm^2 and 6.73 mg/cm^2, respectively. The diameter of the SOC400/SOC650 anode piece is 14 mm. The LCO/SOC400 and LMO/SOC650 cells were assembled in coin-type CR2032 cells in an Ar-filled glovebox. The coating side of LATP@PE and Al_2O_3@PE separator is next to the anode electrode. The electrolyte is 1M $LiPF_6$ in ethylene carbonate/dimethyl carbonate (EC/DMC, 1 : 1 v/v) with addition of 3 wt% fluoroethylene carbonate (FEC).

2.4. Electrochemistry measurements

The charge–discharge cycle performances were measured on a cell testing system (LAND CT2001 A, China). The LCO-SOC400 and LMO-SOC650 cells were charge–discharged in the voltage range of 2.75–4.4 V and 2.75–4.2 V, respectively. The cells were cycled at 0.1 C for the first five cycles and then at 1 C for the subsequent cycles. The electrochemical impedance spectroscopy (EIS) measurements were performed on an electrochemical work station system (ZENNIUM, ZAHNER) with frequencies ranged from 100 kHz to 10 MHz. The AC voltage perturbance is 5 mV.

3. Results and discussion

As LATP is regarded as the essential material to optimize the cell performance, XRD was employed to check the phase purity of LATP (Fig. 1(a)). The XRD pattern is overall consistent with the standard pattern of LATP (PDF: 35-0754), with no notable impurities that can be observed. The sharp XRD peaks indicate the good crystallinity of the as-synthesized

sample. Further Rietveld refinement confirms the pure phase of LATP with a NASICON structure (S.G.R-3c). The morphology of the LATP was characterized by SEM, showing an irregular particle shape with a size distribution in the range of 500–700 nm (see Fig. 1(b)). Al_2O_3 with similar particle size was deliberately chosen to coat the separator for paralleling comparison. Figures 1(c) and 1(d) show the surface morphologies of Al_2O_3@PE and LATP@PE, respectively. Granularity equivalent Al_2O_3 and LATP particles are coated and uniformly distributed on the surface of the PE separator without any aggregation. The thickness of the LATP and Al_2O_3 coating layer was controlled to be around 2 μm.

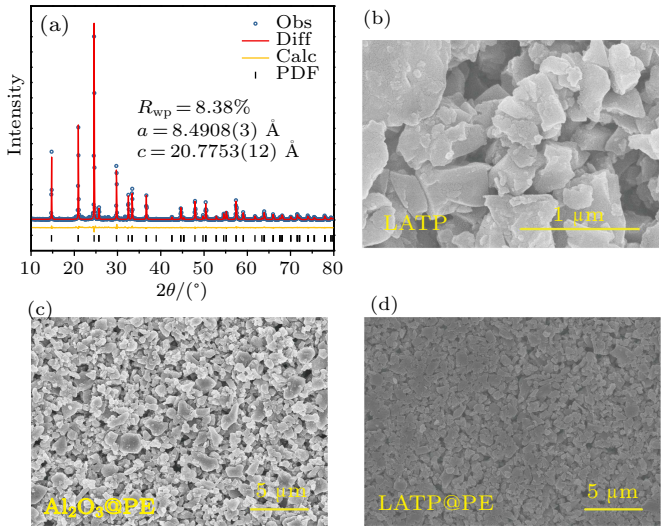

Fig. 1. (a) The XRD pattern and (b) SEM image of the LATP powder. The surface morphologies of (c) Al_2O_3@PE and (d) LATP@PE separators.

To evaluate the effectiveness of the LATP coating on the suppression of TM dissolution, charge–discharge cycle tests were performed. Figures 2(a) and 2(b) display the first cycle charge and discharge curves of the LCO-SOC400 cell and the LMO-SOC650 cell using Al_2O_3 coated and LATP coated separators, respectively. The LCO-SOC400 cell with LATP@PE exhibits higher charge capacities (191.8 mAh/g) and discharge capacities (172.4 mAh/g) than the cell with Al_2O_3@PE which shows the first charge capacities of 184.8 mAh/g and discharge capacities of 167.0 mAh/g. The initial coulombic efficiencies (CEs) are comparable between LCO-SOC400 cells using LATP@PE (89.88%) and Al_2O_3@PE (90.36%), but lower than the CE of $LiCoO_2$ half-cell using Li metal anode. This can be attributed to the formation of a thicker SEI layer on SiO/graphite anode which would consume more lithium ions.[22,23] The LMO-SOC650 cells show a similar charge–discharge behavior. The first charge capacities (122.1 mAh/g) and discharge capacities (89.4 mAh/g) of the LMO-SOC650 cell with LATP@PE are also larger than those with Al_2O_3@PE (118.8 mAh/g and 84.5 mAh/g). The first cycle CEs of the LMO-SOC650 cells (71.12% for LATP@PE and 73.21% for Al_2O_3@PE) are lower than those of the LCO-SOC400 cell, which is due to the higher content of SiO used in SOC650 than SOC400. The above results indicate that, the LATP@PE separator, no matter utilized in LCO-SOC400 or LMO-SOC650 systems, could enable higher first cycle capacities than the Al_2O_3@PE separator counterparts. And the optimized batteries performance is attributed to the different anode/separator interface properties. The in-depth mechanism will be discussed later combining with the multi-faceted characterizations.

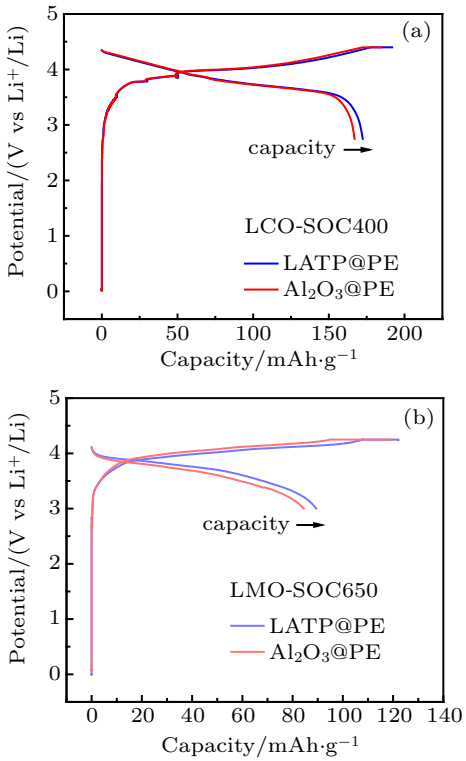

Fig. 2. Charge–discharge curves of (a) LCO-SOC400 cell and (b) LMO-SOC650 cell for the first cycle. The red and blue curves represent the cells using Al_2O_3 coated and LATP coated separators, respectively.

The cycle performances of the LCO-SOC400 and LMO-SOC650 cells using the Al_2O_3@PE and LATP@PE separators were tested at room temperature. All the cells were charge–discharged at 0.1 C-rate for the first 5 cycles (the shadow in Fig. 3(a) contains more than 5 cycles), and then cycled at 1 C-rate for the subsequent cycles. As shown in Fig. 3(a), the LCO-SOC4000 with LATP@PE shows a much better discharge capacity retention (83.23%/50th cycle) than the cell with Al_2O_3@PE (59.57%/50th cycle). Similar behavior can also be observed for LMO-SOC650, where the cell using LATP@PE presents superior capacity retention compared to that using Al_2O_3@PE (73.7% versus 67.45% for 50th cycle). For comparing the capacity retention ability of these two kinds of separators, the capacity evolution ranges from the 1st to the 50th cycle are put together to obtain a clear view (Figs. 3(c) and 3(d)). In general, the cells using LATP@PE separator display a remarkable advantage in the capacity retention ability over the Al_2O_3@PE cells. Specifically, for LCO-SOC400 cells, the LATP@PE cell has the capacity exacerbation from 172.4 mAh/g to 143.4 mAh/g, which is much better than the

Al_2O_3@PE cell. Moreover, the ones using LATP@PE separator manifest a tendency that the capacity fading slows down with a faster speed, which might imply the formation of a more stable SEI layer. These results illustrate that the cycle performances of cells using LATP@PE is better than those using Al_2O_3@PE during the full battery life.

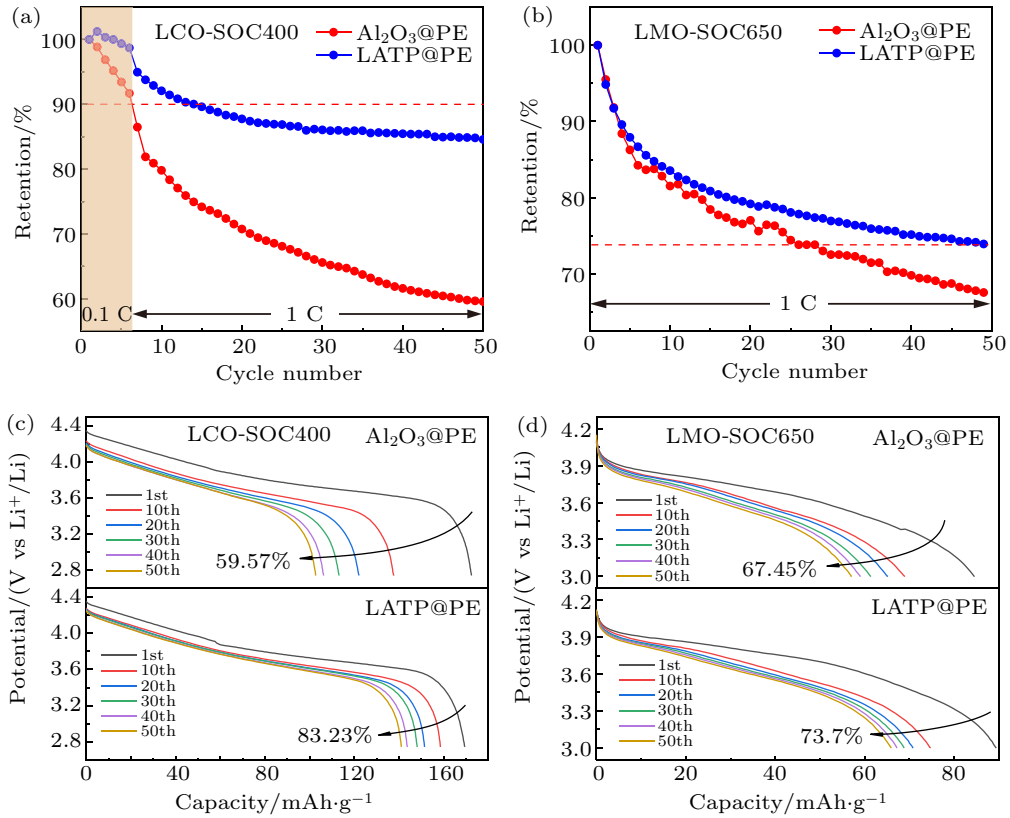

Fig. 3. Discharge capacity retention of (a) LCO-SOC400 cell and (b) LMO-SOC650 cell. Discharge profiles of (c) LCO-SOC400 cells and (d) LMO-SOC650 cells at different cycles.

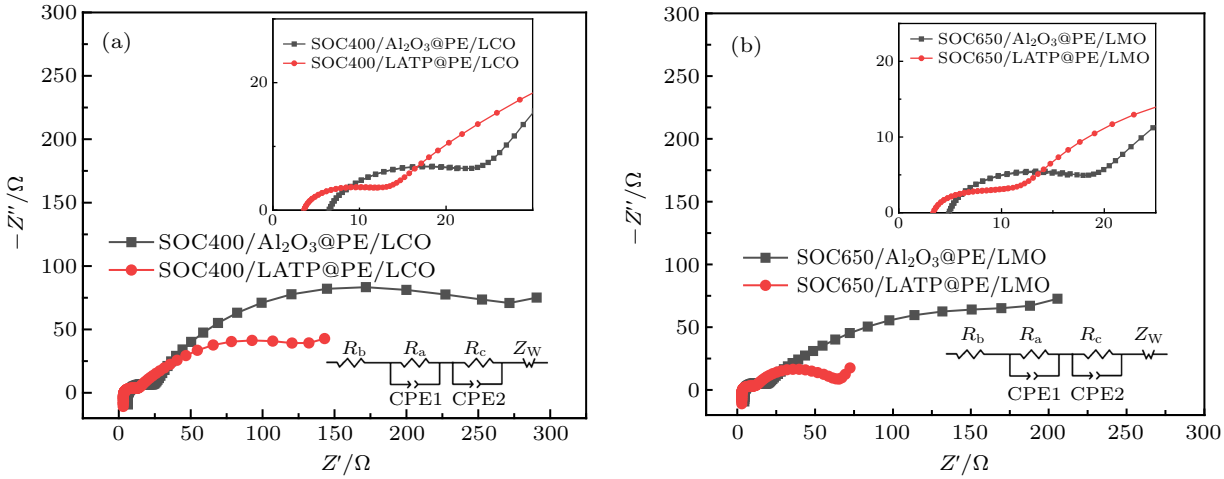

Fig. 4. EIS spectra for (a) the LCO-SOC400 cells and (b) the LMO-SOC650 cells after 50 cycles. R_b: ohmic resistance; R_a: resistance of SEI at anode; R_c: resistance of CEI at cathode; CPE: constant phase element.

To understand the impact of the coating layer on the battery performances, EIS measurements were carried out to inspect the interfacial properties of the cells after electrochemical cycling. While all spectra show a similar line shape with two well-separated semi-circles which can be ascribed to the transport resistances from CEI at cathode side and SEI at anode side (denoted as R_a and R_c), much suppressed intermediate-frequency semi-circles can be observed for both cells using the LATP@PE separator. Considering that the difference comes from the coating layer facing to the anode electrode side, the distinct intermediate-frequency resistance behaviors may be due to the different SEI properties of the cells using LATP@PE separator and Al_2O_3@PE separator. Quantitatively analysis was performed by fitting the spectra with an

equivalent circuit model as depicted in the insets of Figs. 4(a) and 4(b). The detailed results are listed in Table 1. It can be found that the cells using Al_2O_3@PE separator exhibit slightly larger cell ohmic resistance (R_b) and R_c values, but significant larger R_a values than the cells using LATP@PE separator (for LCO cells, 265.7 Ω versus 174.4 Ω; for LMO cells, 270.7 Ω versus 57.0 Ω), indicating the more severe deterioration of the interfacial property for the Al_2O_3@PE cells over the electrochemical cycling. This is also in good consistent with the more rapid decay of the capacity for the Al_2O_3@PE cells.

Since the main differences between the cells come from the different coating layers on the separators, it is rational to extrapolate that there should be evident difference on the actual working part, that is the separator, after battery cycling. We therefore examined the surface morphology of the separators retrieved from the LCO cells after 50 cycles. Interestingly, the surface morphology of Al_2O_3@PE has barely changed after 50 cycles (Figs. 5(a) and 5(b)) comparing to its original one displayed in Fig. 1(c), whereas significant morphology changes can be seen on LATP@PE as shown in Figs. 5(c) and 5(d) (SEM image of the original LATP@PE is shown in Fig. 1(d)). It can be seen that, a dense interphase layer is formed on the surface of the PE separator, replacing the originate-state LATP particles. Meanwhile, some cracks are also found which may be caused by stress accumulation and volume change. As it is well-known that LATP can be reduced at low voltage (2.5 V vs. Li/Li^+),[24,25] the formation of the dense interphase layer should be owing to the reduction of LATP particles during the discharge process. Besides, the volume expansion after the interphase formation was also reported by Lewis *et al.*,[26] which is well consistent with our SEM observations.

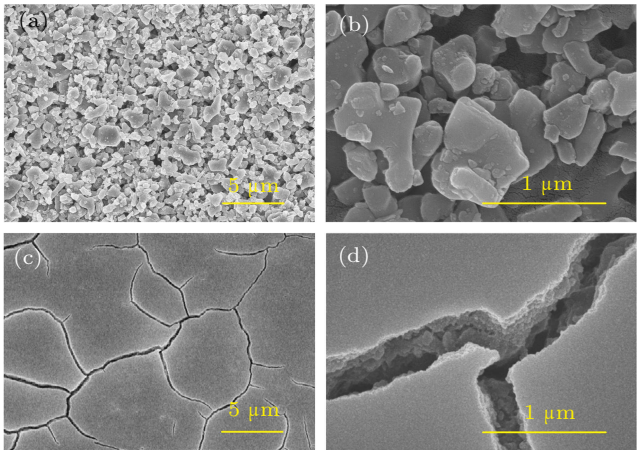

Fig. 5. SEM images of (a), (b) Al_2O_3@PE and (c), (d) LATP@PE separators retrieved from the cells after 50 cycles.

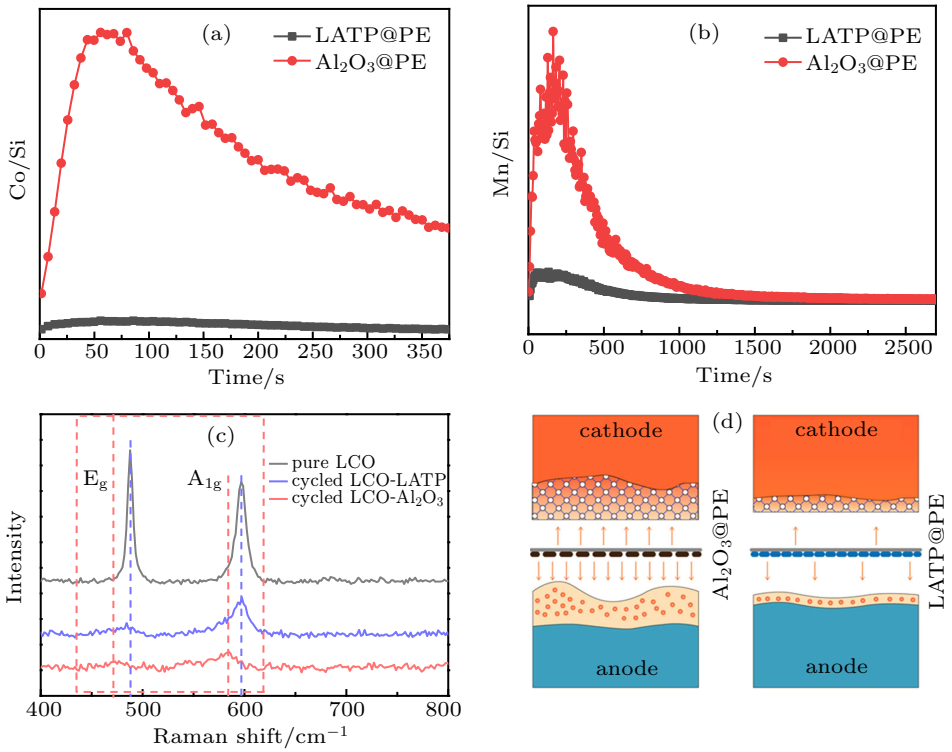

Fig. 6. SIMS profiles collected on the anode electrodes retrieved from (a) LCO-SOC400 cell and (b) LMO-SOC650 cell after 50 cycles. (c) Raman spectra of LCO electrodes retrieved from LCO-SOC400 with LATP@PE and Al_2O_3@PE separators. (d) Schematic illustration of the TM dissolution and decomposition process.

The cathode and anode electrodes were harvested from the LCO-SOC400 and LMO-SOC650 cells after 50 cycles. The transition metal element content was detected by SIMS on the anode electrodes after DMC washing and drying. The signal of silicon was chosen as a reference signal because of its consistency during the charge–discharge process. It can be inferred from Figs. 6(a) and 6(b) that the ratio of TM/Si of Al_2O_3@PE cells is much higher than that of LATP@PE, both

in the LCO-SOC400 cell and the LMO-SOC650 cell, suggesting the much more suppressed TM deposition on the anode electrodes for the cells with LATP@PE than with Al_2O_3@PE. Raman spectroscopy measurements were performed to inspect the surface structure change of $LiCoO_2$ after cycling. A relative weak spectrum signal of the Al_2O_3@PE cell indicates the more severe surface structure deconstruction than the LCO electrode in LATP@PE cells. The existence of the characteristic peaks (E_g and A_{1g} vibration modes in $LiCoO_2$) suggests the preservation of the main $LiCoO_2$ layered structure, while the overall suppressed spectrum intensity, for LCO from the Al_2O_3@PE cell, can be attributed to destruction of the $LiCoO_2$ surface, indicating the more severe Co dissolution.[27,28] Combining with the aforementioned EIS and SEM results, it can be learned that the reaction of the LATP during battery cycling (very likely the first several cycles) renders the formation of a uniform and dense interphase layer, which can effectively prevent the deposition of TM on the anode electrode. As the catalytic effect of the deposited TM is known to be one of the main causes for the growth of SEI layer, the inhibition of the TM deposition may contribute to the substantially enhanced interfacial stability for cells using Al_2O_3@PE separator over the cycling process. Moreover, since "consumption" of the TM at the anode side is suppressed, the demand for the "supply" from the cathode is also reduced, and therefore, the TM dissolution from the cathode is greatly inhibited. All these benefits synergistically contribute to the much more enhanced cycle stability for the cells using LATP@PE separator.

4. Conclusion and perspectives

In the present work, we demonstrate that a LATP coating layer on the polymer separator can inhibit the undesired transition metal dissolution and deposition process in LIBs. By using various characterizations such as SEM, SIMS, and Raman, it is revealed that the surface morphology of the LATP coating layer has been significantly changed owing to the reduction of LATP at the discharge process. The as-formed dense surface layer can effectively prevent the TM deposition on the anode electrode and inhibit the TM dissolution from the cathode electrode. Besides, the as described TM block function of the LATP@PE separator is mainly attributed to the *in situ* formed interphase, which is formed by the reduction of LATP under low potential, thus the LATP@PE separator can work with various anodes. As a result, the deconstruction of the cathode material and the deterioration of the electrolyte/anode interface can be largely suppressed. The cells using LATP coated separator show superior cycle performances to the cells using regular Al_2O_3 coated separator. This work demonstrates that the functional coating on the separator, in addition to the traditional strategies through modifications of the cathode materials, can effectively solve the TM dissolution and deposition problem, which is one of the most critical issues that should be addressed to improve the long-term cycle stability of LIBs.

Table 1. The detailed results of fitting the spectra with an equivalent circuit model.

Sample	R_b/Ω	R_c/Ω	R_a/Ω
LCO-SOC400 with LATP@PE	3.6	7.1	174.4
LCO-SOC400 with Al_2O_3@PE	6.6	15.1	265.7
LMO-SOC650 with LATP@PE	3.4	6.5	57.0
LMO-SOC650 with Al_2O_3@PE	4.9	10.2	270.7

References

[1] Armand M and Tarascon J M 2008 *Nature* **451** 652
[2] Liang Y, Zhao C Z, Yuan H, Chen Y, Zhang W, Huang J Q, Yu D, Liu Y, Titirici M M, Chueh Y L, Yu H and Zhang Q 2019 *Infomat* **1** 6
[3] Liu C, Li F, Ma L P and Cheng H M 2010 *Adv. Mater.* **22** E28
[4] Li W Z, Wang Z, Ban L, Wang J and Lu S 2019 *Acta Chim. Sin.* **77** 1115
[5] Zhan C, Wu T, Lu J and Amine K 2018 *Energy Environ. Sci.* **11** 243
[6] Zhang X Q, Wang X M, Li B Q, Shi P, Huang J Q, Chen A and Zhang Q 2020 *J. Phys. Chem. A* **8** 4283
[7] Zhou G, Sun X, Li Q, Wang X, Zhang J, Yang W, Yu X, Xiao R J and Li H 2020 *J. Phys. Chem. Lett.* **11** 3051
[8] Tang D, Sun Y, Yang Z, Ben L, Gu L and Huang X 2014 *Chem. Mater.* **26** 3535
[9] Wang L F, Ou C C, Striebel K A and Chen J S 2003 *J. Electrochem. Soc.* **150** A905
[10] Delacourt C, Kwong A, Liu X, Qiao R, Yang W L, Lu P, Harris S J and Srinivasan V 2013 *J. Electrochem. Soc.* **160** A1099
[11] Zhan C, Lu J, Jeremy Kropf A, Wu T, Jansen A N, Sun Y K, Qiu X and Amine K 2013 *Nat. Commun.* **4** 2437
[12] Qian Y, Kang Y, Hu S, Shi Q, Chen Q, Tang X, Xiao Y, Zhao H, Luo G, Xu K and Deng Y 2020 *ACS Appl. Mater. Interfaces* **12** 10443
[13] Gutierrez A and Manthiram A 2013 *J. Electrochem. Soc.* **160** A901
[14] Hou Y, Chang K, Tang H, Li B, Hou Y and Chang Z 2019 *Electrochim. Acta* **319** 587
[15] Fu L J, Liu H, Li C, Wu Y P, Rahm E, Holze R and Wu H Q 2006 *Solid State Sci.* **8** 113
[16] Warburton R E, Young M J, Letourneau S, Elam J W and Greeley J 2020 *Chem. Mater.* **32** 1794
[17] Yamane H, Inoue T, Fujita M and Sano M 2001 *J. Power Sources* **99** 60
[18] Zhou H M, Liu B, Xiao D M, Yin C J and Li J 2019 *J. Mater. Sci.: Mater. Electron.* **30** 5098
[19] Banerjee A, Ziv B, Shilina Y, Luski S, Aurbach D and Halalay I C 2017 *ACS Energy Lett.* **2** 2388
[20] Manthiram A, Yu X and Wang S 2017 *Nat Rev. Mater.* **2** 16103
[21] Yang Q, Huang J, Li Y, Wang Y, Qiu J, Zhang J, Yu H, Yu X, H Li H and Chen L 2018 *J. Power Sources* **388** 65
[22] Lee J K, Lee J H, Kim B K and Yoon W Y 2014 *Electrochim. Acta* **127** 1
[23] Zhao J, Lee H W, Sun J, Yan K, Liu Y, Liu W, Lu Z, Lin D, Zhou G and Cui Y 2016 *Proc. Natl. Acad. Sci. USA* **113** 7408
[24] Liu L, Zhou M, Wang G, Guo H, Tian F and Wang X 2012 *Electrochim. Acta* **70** 136
[25] Luo J Y, Chen L J, Zhao Y J, He P and Xia Y Y 2009 *J. Power Sources* **194** 1075
[26] Lewis J A, Cortes F J Q, Boebinger M G, Tippens J, Marchese T S, Kondekar N, Liu X, Chi M and McDowell M T 2019 *ACS Energy Lett.* **4** 591
[27] Le Van-Jodin L, Rouchon D, Le V H, Chevalier I, Brun J and Secouard C 2019 *J. Raman Spectrosc.* **50** 1594
[28] Matsuda Y, Kuwata N, Okawa T, Dorai A, Kamishima O and Kawamura J 2019 *Solid State Ion.* **335** 7